

# Cathodoluminescence and Photoluminescence Studies of Undoped and $\text{Eu}^{2+}$ Doped $\text{SrAl}_2\text{O}_4$ Phosphors Prepared by Combustion Method

M. Nazarov<sup>a,\*</sup> and D. Spassky<sup>b,c</sup>

<sup>a</sup> Institute of Applied Physics, Moldova State University, Chisinau, MD-2028 Moldova

<sup>b</sup> Skobeltsyn Institute of Nuclear Physics, Lomonosov Moscow State University, Moscow, 11999 Russia

<sup>c</sup> Institute of Physics, University of Tartu, Tartu, 50411 Estonia

\*e-mail: mvnazarov@mail.ru

Received March 25, 2023; revised May 22, 2023; accepted May 22, 2023

**Abstract**—Undoped and  $\text{Eu}^{2+}$  doped strontium aluminate ( $\text{SrAl}_2\text{O}_4$ ) nanosized phosphorescent powders were prepared by urea-nitrate solution combustion method at  $500^\circ\text{C}$  for 5 minutes. The average particle size of the powders was about 60 nm. The photoluminescent properties have been studied using the synchrotron radiation and electron excitation. The broad photoluminescence bands were observed in  $\text{SrAl}_2\text{O}_4:\text{Eu}^{2+}$  peaking at  $\lambda_{\text{max}} = 450$  and 525 nm, which arise due to transitions from the  $4f^65d^1$  to  $4f^7$  configuration of the  $\text{Eu}^{2+}$  ions situated in two sites with different symmetry. Three additional emission bands were also observed at 250, 370 and 403 nm in undoped as well as  $\text{Eu}$ -doped samples. The bands are attributed to the intrinsic emission of self-trapped excitons (band at 250 nm) and to extrinsic emission from complexes containing structural defects (bands at 370 and 403 nm).

**Keywords:**  $\text{SrAl}_2\text{O}_4$ ,  $\text{SrAl}_2\text{O}_4:\text{Eu}^{2+}$ , cathodoluminescence, photoluminescence, synchrotron radiation

**DOI:** 10.1134/S1027451023050282

## 1. INTRODUCTION

Until recent decade, strontium aluminate phosphors doped with europium ions have attracted much attention since they show excellent properties as persistent phosphors. The study of the luminescent properties of  $\text{SrAl}_2\text{O}_4:\text{Eu}^{2+}$  has been the subject of a large number of both experimental and theoretical works as well as numerous reviews [1–8]. Their number is increasing every year, since not all the observed phenomena have found their explanation.

The main works in this area are based on the application of photoluminescent methods in the UV range and the explanation of the nature of the main emission bands at 450 and 525 nm. Usually the experiments were carried out under excitation in UV spectral region up to 6 eV. The application of high-energy excitation sources such as synchrotron radiation as well as electron beams, makes it possible to significantly supplement the observed picture. Previously it allowed us to detect additional emission bands in UV spectral range. In particular, an additional emission band at 250 nm was detected under interband VUV excitation and ascribed to intrinsic emission [9]. However, for other UV emission bands the origin of emission cen-

ters is still not fully understood, and it is under discussion.

The aim of this work is to study the properties of  $\text{SrAl}_2\text{O}_4$ , undoped as well as doped with  $\text{Eu}^{2+}$  synthesized by the combustion method with a lower combustion temperature in order to produce nanoparticle powder for further study of the nature of the UV emission bands. We continue our works in this area and prepared new samples, which differed from the previous ones in modified synthesis parameters and conditions. Experimental measurements were carried out under excitation with synchrotron radiation in broad energy range 4.5–25 eV as well as electron excitation.

## 2. EXPERIMENTAL SECTION

### 2.1. Sample Preparation

$\text{SrAl}_2\text{O}_4:\text{Eu}^{2+}$  phosphor was prepared by combustion synthesis. The starting material included Aluminum nitrate ( $\text{Al}(\text{NO}_3)_3 \cdot 9\text{H}_2\text{O}$ ; System, 98%), strontium nitrate ( $\text{Sr}(\text{NO}_3)_2$ ; Aldrich, 99%), europium oxide ( $\text{Eu}_2\text{O}_3$ ; Aldrich, 99.99%) and urea ( $\text{CO}(\text{NH}_2)_2$ ; System, 99%). Small amount of acid boric ( $\text{H}_3\text{BO}_3$ ; Fisher, 100.04%) were used as flux and small amounts

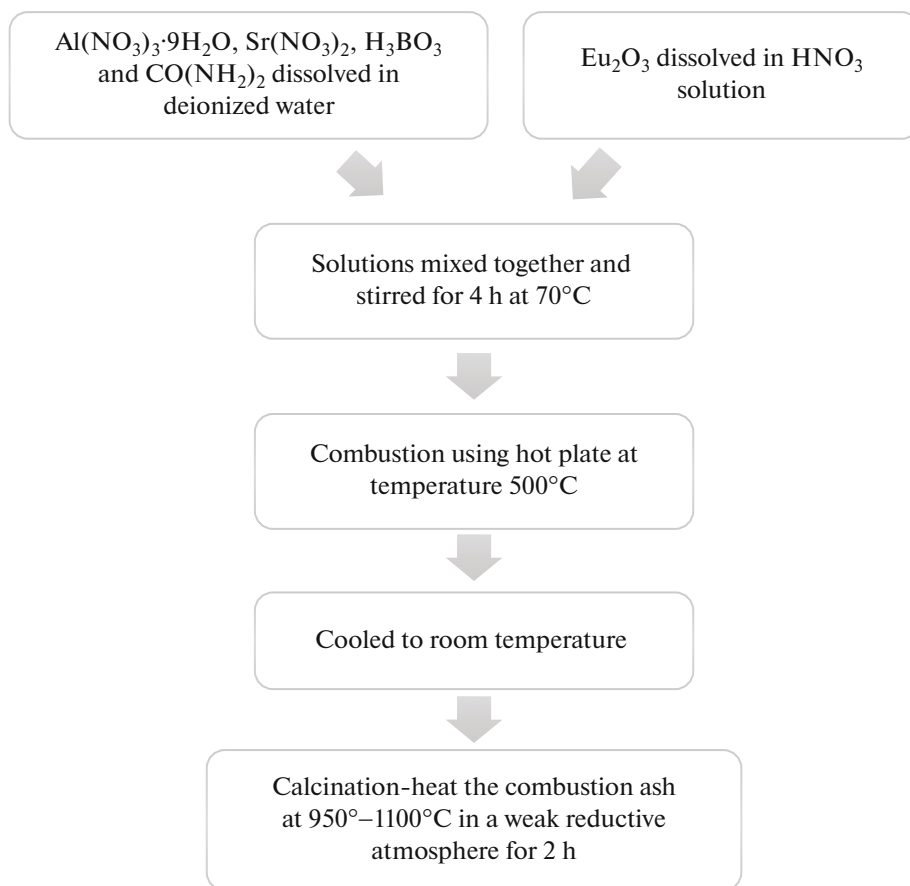
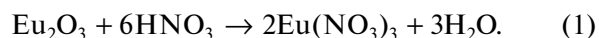


Fig. 1. Flow chart of  $\text{SrAl}_2\text{O}_4:\text{Eu}^{2+}$  phosphors powder by combustion synthesis.

of urea were used as reducer and fuel. Figure 1 shows the flow chart of  $\text{SrAl}_2\text{O}_4:\text{Eu}^{2+}$  powders synthesis.

There are four stages to describe the combustion synthesis:

**Stage I: Composition of raw materials.** The stoichiometric quantities of raw materials were calculated and weighed by using high precision mass balance. The composition of the acid boric was set as 0.08 mol %. Raw materials of  $\text{Al}(\text{NO}_3)_3 \cdot 9\text{H}_2\text{O}$ ,  $\text{Sr}(\text{NO}_3)_2$ ,  $\text{H}_3\text{BO}_3$  and  $\text{CO}(\text{NH}_2)_2$  were dissolved into 20 ml of deionized water respectively to obtain transparent solution. Wet mixing was used to obtain homogeneous mixture. Deionized water is selected instead of distilled water due to the removal of the mineral ions such as cations from sodium, calcium, iron, copper and anions from chloride and bromide which will influence on the experiment result [10].  $\text{Eu}_2\text{O}_3$  was dissolved with minimum amount of  $\text{HNO}_3$  solution to convert into  $\text{Eu}(\text{NO}_3)_3$  according to the equation (1):

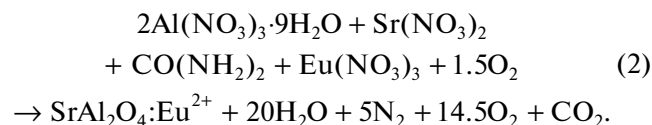


**Stage II: Mixing.** These two solutions were mixed together and stirred using magnetic bar for several hours at  $75^\circ\text{C}$  to obtain viscous gel solution. The mix-

ing temperature was set at the range between 70 to  $80^\circ\text{C}$  due to several reasons. Firstly, according to the MSDS, Aluminum nitrate has a fairly low melting point ( $73^\circ\text{C}$ ) but a high boiling point or decomposition temperature ( $135^\circ\text{C}$ ). The heating of aluminum nitrate above its melting point encourages the formation of a homogeneous solution. Furthermore, it can dissolve acid nitric, which has a low boiling point ( $83^\circ\text{C}$ ).

**Stage III: Combustion synthesis.** The mixed viscous gel obtained continues for combustion reaction. The combustion is done by using a hot plate instead of furnace. White combustion ash was obtained in 3–5 min by combusting the precursor gel at temperature  $500^\circ\text{C}$ . Initially, the solution boiled and underwent dehydration followed by decomposition with emission of large amounts of gasses (oxides of carbon, nitrogen and ammonia). Later, the viscous gels spontaneously start to burn and burn slowly without flame (smouldering combustion), thus producing white fined powder. The whole process takes less than 5 minutes. When heated at  $500^\circ\text{C}$ , the powder was held for a few minutes to ensure the combustion reaction was complete. The chemical equation of combustion is compli-

cated and not yet verified; however, the brief equation can be shown as follows:



Next, the combustion ash was cooled to room temperature.

**Stage IV: Calcinations step.** The final pigments synthesis is done by heating the combustion ash at 950–1100°C in a weak reductive atmosphere for 2 h to obtain  $\text{SrAl}_2\text{O}_4:\text{Eu}^{2+}$  phosphor. The weak reductive atmosphere was created by using graphite crucible to inhibit further oxidation.

## 2.2. Characterization Techniques

**X-ray diffraction (XRD).** Phase identification was carried out using a Bruker diffractometer. D8 Advance X-ray Diffraction (XRD) instrument with  $\text{CuK}\alpha$  radiation of wavelength 1.54 Å was applied. Data were collected by step-scanning  $2\theta$  from 10° to 90° and 0.034 s counting time at each step at room temperature.

**Scanning electron microscopy (SEM).** The morphology and topography of the samples were observed by using scanning electron microscope (SEM) Zeiss Supra 35 VP in Secondary Electron (SE) image mode with accelerating voltages: 0.1–30 by 0.01 kV steps and Magnifications: 12×–900.000×. The samples were coated with a few nanometers thick gold palladium layer by using Sputter Coater Polaron SC 515 before SEM observation.

**Photon cross-correlation spectroscopy (PCCS).** The particle sizes of samples were determined by NANOPHOX (NX0064) Particle Size Analyzer in the range of about 1 nm to 10 μm in opaque suspensions and emulsions. For the sample preparation a small amount of the powder was dispersed in deionized water and stirred for 15 minutes, using a magnetic bar. Then, ultrasonic bath was used for vibrating during next 15 minutes before the measurements.

**Photoluminescence (PL).** The measurements of luminescence and luminescence excitation spectra were performed using synchrotron radiation (SR) in UV–VUV energy regions at the branch-line FINEST (energy region 4–25 eV) at MAX-lab, Lund [11]. The excitation spectra were corrected using sodium salicylate. The luminescence spectra were measured with ARC Spectra Pro 300i monochromator equipped with Hamamatsu H6240-01 photon counting head. The samples were mounted on the cold finger of a liquid He flow cryostat and the spectra were recorded in the temperature range 5–300 K.

**Cathodoluminescence (CL).** The measurements of cathodoluminescence spectra were performed under irradiation with electrons (5 keV, 0.4 μA, spot ~1 mm<sup>2</sup>). All measurements were carried out in a liq-

uid helium vacuum cryostat (5–400 K temperature range,  $2 \times 10^{-7}$  Torr vacuum) equipped with Lake Shore 331 Temperature Controller. The luminescence was detected using the UV–VIS–NIR (200–1700 nm) monochromator ARC SpectraPro-2300i equipped with Hamamatsu photon counting head H6240. Emission spectra were not corrected on the sensitivity function of registration channel.

## 3. RESULTS AND DISCUSSION

### 3.1. Structure and Morphology

**XRD analysis.** A typical X-ray diffraction pattern of the resultant  $\text{SrAl}_2\text{O}_4:\text{Eu}^{2+}$  and  $\text{SrAl}_2\text{O}_4$  powders are shown in Fig. 2.  $\text{SrAl}_2\text{O}_4$  powders are all characterized by low-temperature monoclinic phase ( $\alpha$ -phase), lattice constants are  $a = 8.442 \text{ \AA}$ ,  $b = 8.822 \text{ \AA}$ ,  $c = 5.160 \text{ \AA}$ ,  $\beta = 93.415^\circ$ . The synthesized phosphor's (SAE phosphor) dominating peaks are completely matches that of the reference JCPDS Card 01-074-0794. The XRD pattern indicate that no significant change in the host crystal occurred due to the doping with  $\text{Eu}^{2+}$ . Generally, it can be assumed that  $\text{Eu}^{2+}$  ions enter into the  $\text{Sr}^{2+}$  ion sites in the  $\text{SrAl}_2\text{O}_4$  host because the radii of  $\text{Eu}^{2+}$  (1.17 Å) ions are similar to that of the  $\text{Sr}^{2+}$  ions (1.18 Å). Therefore, their substitutions may not generate a significant distortion of the lattice parameter. However, one of the intensive peaks (~32°) does not coincide with the monoclinic  $\text{SrAl}_2\text{O}_4$  ICDD data and corresponds to cubic phase  $\text{Sr}_3\text{Al}_2\text{O}_6$  ( $a = b = c = 15.844 \text{ \AA}$ ). The intensity of this peak is higher in the undoped  $\text{SrAl}_2\text{O}_4$  crystal than in  $\text{Eu}^{2+}$  doped  $\text{SrAl}_2\text{O}_4$  crystal (Fig. 2).

**SEM analysis.** In order to determine the morphology and estimate the size and particle distribution, as well as observe the crystallize phases, scanning electron microscopy measurements were carried out. Figure 3 displays typical SEM images of the prepared phosphors.

This is a typical morphology for such high-temperature, combustion-synthesized samples and is the result of the high temperatures developed within a short period of time and a large volume of evolved gases. The phosphor powders are irregular needle-like particles before the calcination and flower-like particles after calcination, the surfaces of the foams show a lot of cracks, voids and pores formed by the escaping gases during combustion reaction.

The possible mechanism of the flower-like structure can be described as shown in Fig. 4. Generally, the crystal growth process involves two parts: nucleation and growth. The particles undergo nucleation at the initial state. With the increase of temperature, the grains become compressed and more fined. The needle shape and star-like structure appear after 500°C. This structure is unstable and agglomerate during cal-

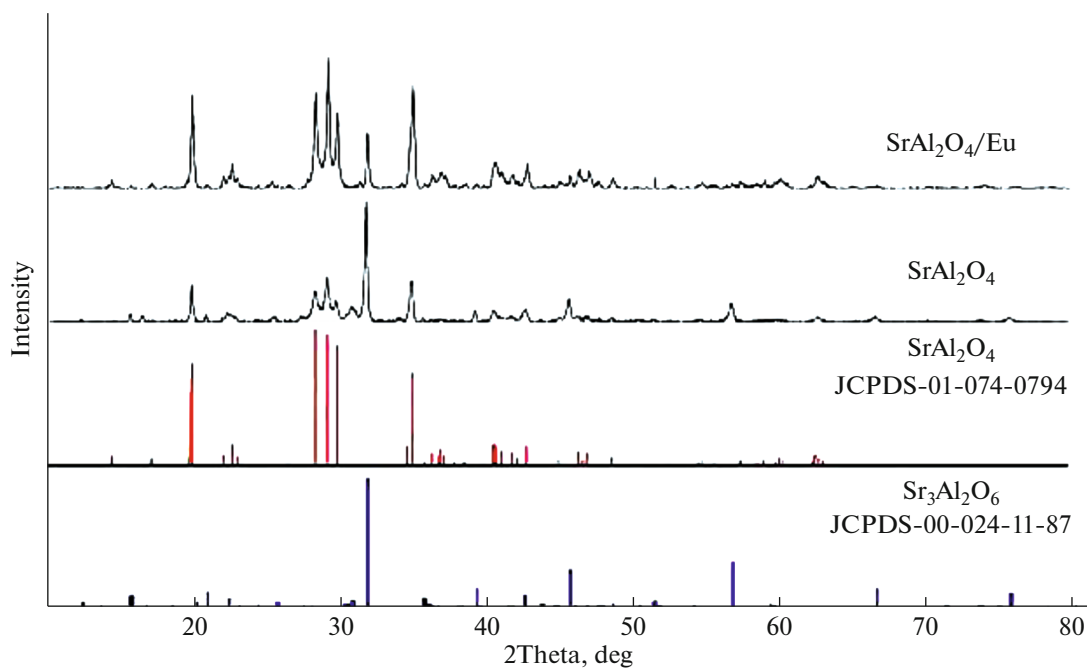


**Fig. 2.** XRD patterns of SrAl<sub>2</sub>O<sub>4</sub> and SrAl<sub>2</sub>O<sub>4</sub>:Eu<sup>2+</sup> phosphors and PDF Cards No. JCPDS-01-074-0794, JCPDS-01-024-11-87.

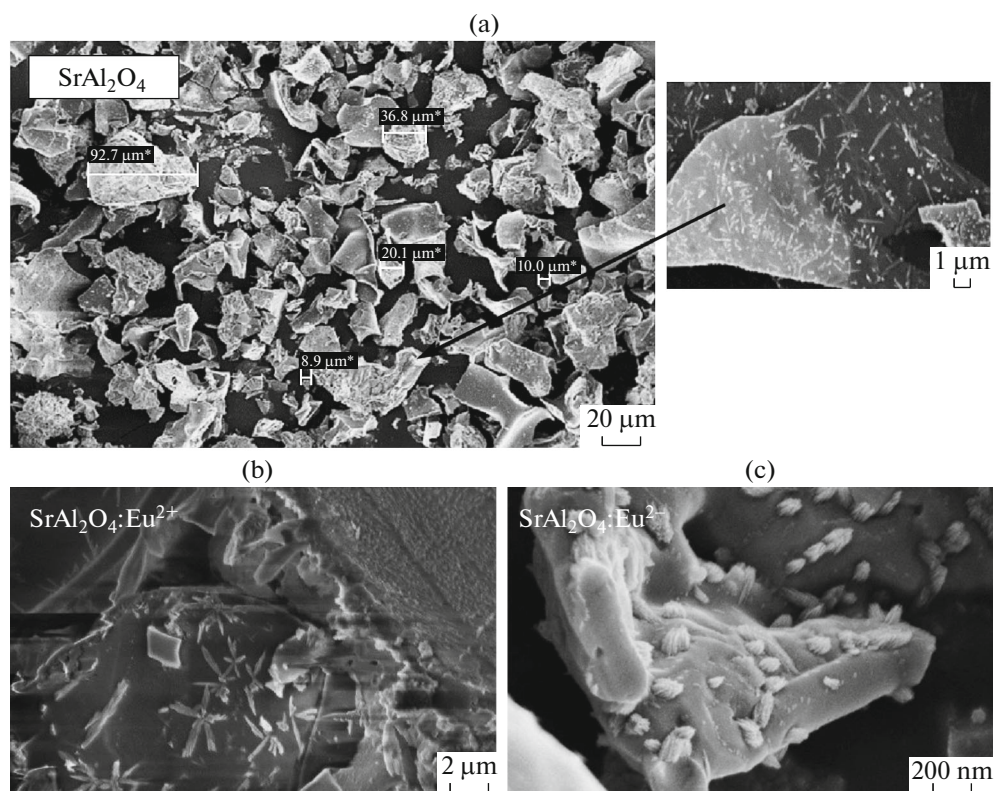


**Fig. 3.** Sample SrAl<sub>2</sub>O<sub>4</sub> before calcination (a), Sample SrAl<sub>2</sub>O<sub>4</sub>:Eu<sup>2+</sup> before calcination (b) and Sample SrAl<sub>2</sub>O<sub>4</sub>:Eu<sup>2+</sup> after calcination at temperature 1000°C (c).

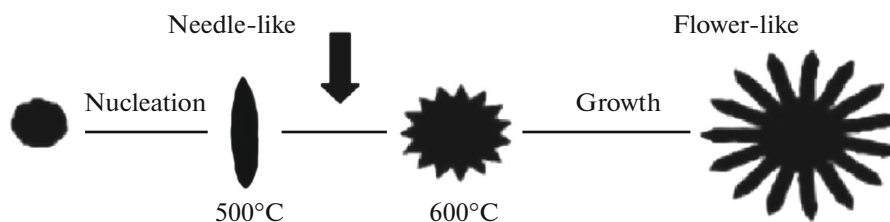


Fig. 4. Scheme illustration of possible mechanism of the flower-like structure  $\text{SrAl}_2\text{O}_4:\text{Eu}^{2+}$  [12].

cinations at  $1000^\circ\text{C}$  to form a stable specific flower-like structure [12, 13].

**Particle size analysis.** The results of particle size measurements are given in Fig. 5 and Table 1.

The results show that all the samples achieve nanoparticle size except for sample  $\text{SrAl}_2\text{O}_4:\text{Eu}^{2+}$  after calcination. For this sample, we observed an increase in the particle size after heating at a higher temperature due to grain grow. Excessive sintering and aggregation of particles occurs, and thus the particle size increases.

### 3.2. PL and CL Spectroscopy

The emission spectra of  $\text{SrAl}_2\text{O}_4:\text{Eu}^{2+}$  under excitation with synchrotron radiation are presented for  $T = 13$  and  $300$  K in Figs. 6a, 6b. The excitation energies were chosen to correspond to interband ( $E_{\text{ex}} = 7.5$  eV) as well as intraband ( $E_{\text{ex}} = 6.1$  eV) electron transitions in  $\text{SrAl}_2\text{O}_4$  taking into account the bandgap value  $E_{\text{g}} = 6.9$  eV. Four emission bands peaking at 520, 450, 360 and 250 nm were observed at low temperatures under interband excitation. The bands at 520 and 450 nm are well known and, after numerous discussions, it is generally accepted that they correspond to electron transitions in  $\text{Eu}^{2+}$  ions, which replaces, respectively, strontium in positions 1 and 2. The difference in the bond lengths for  $\text{Sr}_1$  and  $\text{Sr}_2$  sites can give rise to an essential difference in the position of emission bands as well as structure of excitation spectra [16]. As excitation energy exceeds the band gap in  $\text{SrAl}_2\text{O}_4$ , the peak at 250 nm is observed as well, which corresponds to a radiative annihilation of the intrinsic emission of self-trapped excitons [9]. The UV band at 370 nm (labeled as band 1) remains unexpected and still incomprehensible. Under intraband excitation two bands at 520 and 450 nm related to  $\text{Eu}^{2+}$  were observed

as well as an additional peak at 595 nm. The latter peak is associated with the emission from traces of  $\text{Eu}^{3+}$  ions, which are also presented in the sample. Moreover, an additional emission band presented by a short wavelength shoulder of the emission band at 450 nm has been observed as well (labeled as band 2). This band is clearly observed at higher temperatures ( $T = 300$  K) peaking at 403 nm when the emission band at 450 nm is thermally quenched [15]. The band 1 is detected as well, however its intensity is very low due to thermal quenching and it can be observed when the spectra are plotted in semi logarithmic scale.

Additionally, to find out the origin of UV luminescence bands, CL spectra were measured under irradiation of the sample with high energy electrons (5 keV) (Fig. 7). Beside the well-known peaks at 450 and 520 nm related to  $\text{Eu}^{2+}$ , an additional non-elementary band was observed also at CL in the range 300–400 nm that is supposed to be the superposition of band 1 and band 2. It is worth noting that CL degradation occurs due to charging of the sample. However, the bands at 300–400, 450 and 520 nm, as well as the  $\text{Eu}^{3+}$  related peak at 612 nm, are clearly visible.

The energies of  $5d$   $\text{Eu}^{2+}$  levels due to overall crystal field splitting in  $\text{SrAl}_2\text{O}_4:\text{Eu}^{2+}$  were calculated in our previous work [16] and estimated (in eV) as: 3.10, 3.74, 4.40, 4.52, 6.25 (for  $\text{Eu}^{2+}$  at  $\text{Sr}_1$  site) and 3.30, 3.42, 4.56, 5.64, 6.03 (for  $\text{Eu}^{2+}$  at  $\text{Sr}_2$  site). The energy positions of the split levels are in good agreement with the experimental CL spectra given in Fig. 8. The luminescence mechanism of  $\text{SrAl}_2\text{O}_4:\text{Eu}^{2+}$  is explained as electron transitions from the lowest  $5d$  levels of  $\text{Eu}^{2+}$  ions at  $\text{Sr}_1$  and  $\text{Sr}_2$  positions. The  $\text{Eu}^{2+}$  ions entering the  $\text{Sr}_1$  sites show broad emission at lower energy (at 520 nm), and those ions at the  $\text{Sr}_2$  sites cause the high energy band at 450 nm. The lowest energy level 3.1 eV

Table 1. Particle size analysis data for samples  $\text{SrAl}_2\text{O}_4$ ,  $\text{SrAl}_2\text{O}_4:\text{Eu}^{2+}$  before and  $\text{SrAl}_2\text{O}_4:\text{Eu}^{2+}$  after calcination at  $1000^\circ\text{C}$

Samples	$x_{10}$ , nm	$x_{50}$ , nm	$x_{90}$ , nm	SMD, nm	VMD, nm
$\text{SrAl}_2\text{O}_4$	81.19	84.14	89.39	84.54	84.61
$\text{SrAl}_2\text{O}_4:\text{Eu}^{2+}$	44.15	51.62	60.02	51.27	51.98
$\text{SrAl}_2\text{O}_4:\text{Eu}^{2+}$ ( $1000^\circ\text{C}$ )	112.65	132.21	154.26	131.29	133.20

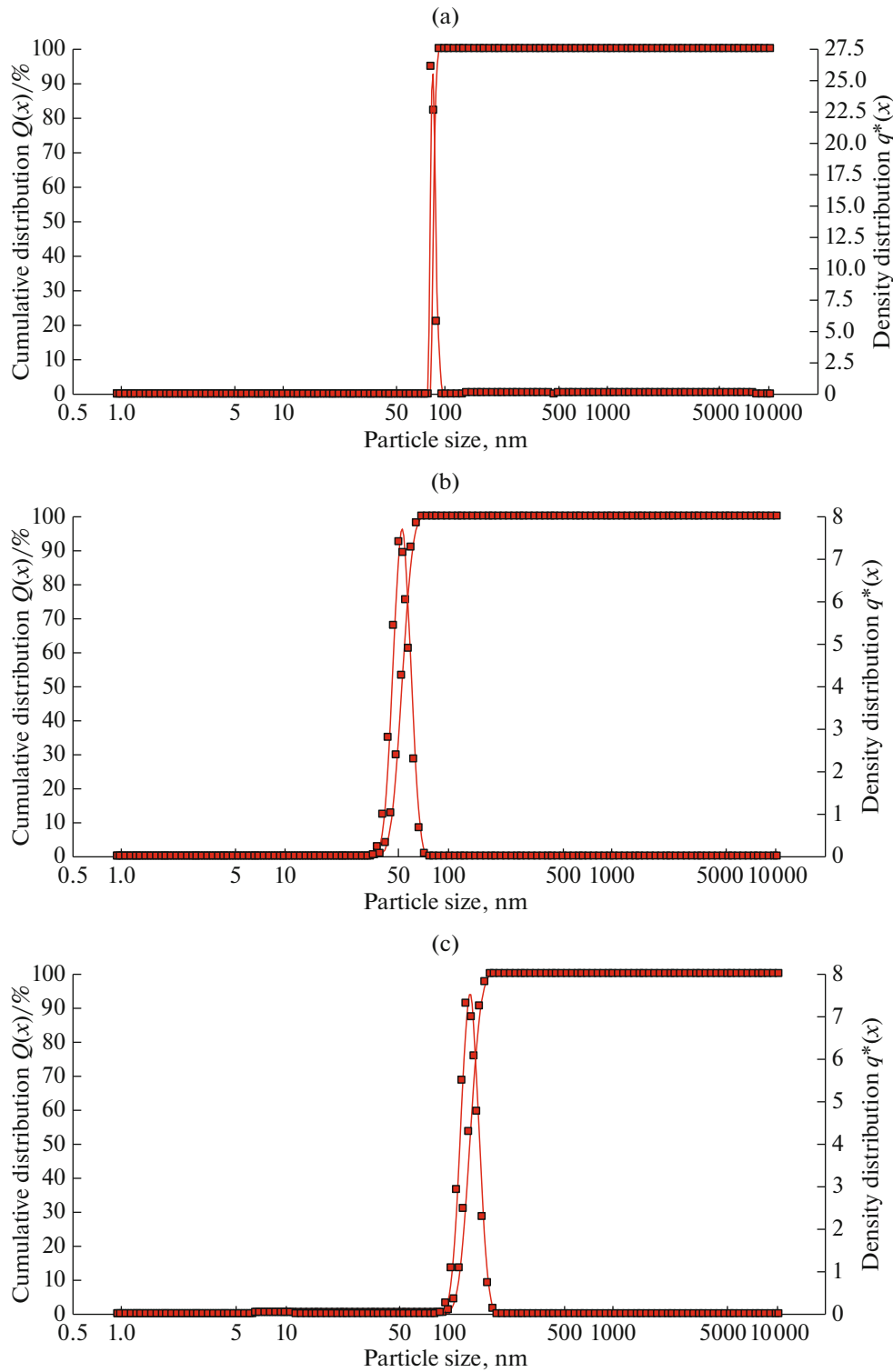


**Fig. 5.** Graph of particle size analysis for samples:  $\text{SrAl}_2\text{O}_4$  (a),  $\text{SrAl}_2\text{O}_4:\text{Eu}^{2+}$  (b) before and  $\text{SrAl}_2\text{O}_4:\text{Eu}^{2+}$  (c) after calcination at  $1000^\circ\text{C}$ .

in  $\text{Sr}_1$  position is responsible for the green luminescence and lowest energy level 3.3 eV in  $\text{Sr}_2$  position is responsible for the blue luminescence.

The origin of the emission bands at 370 and 403 nm is still under discussion. The band at 370 nm could be due to the transition of electrons from the next split

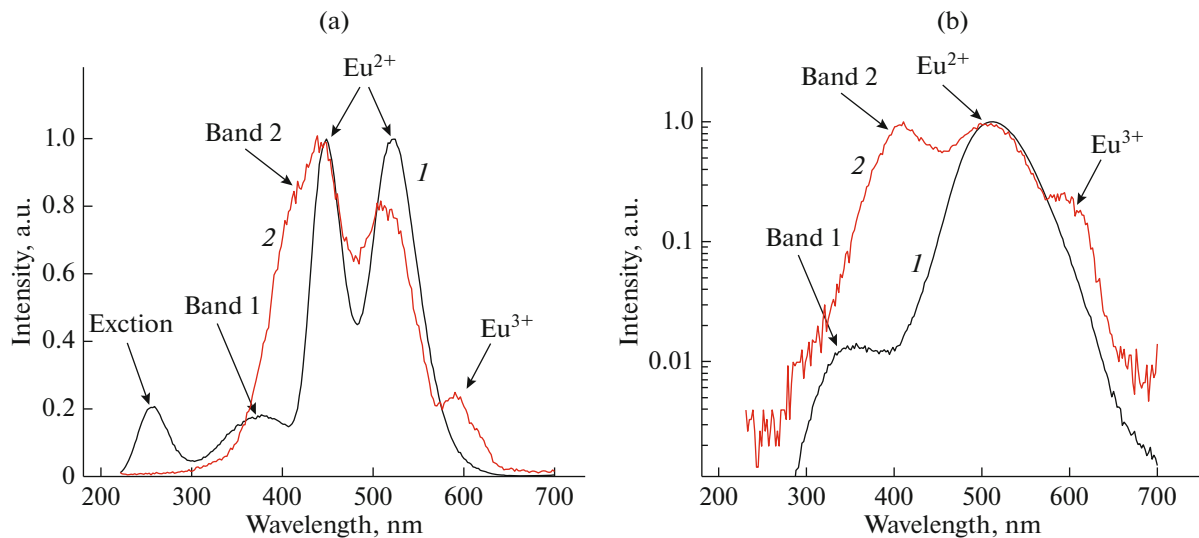


**Fig. 6.** Photoluminescence spectra of the  $\text{SrAl}_2\text{O}_4:\text{Eu}^{2+}$  at  $E_{\text{ex}} = 7.5$  eV (1) and  $E_{\text{ex}} = 6.1$  eV (2),  $T = 13$  K (a) and 300 K (b).

level of europium in the state of  $\text{Sr}_1$ , as the energy of transition coincides with the corresponding energy level. However, such transition might be low probable due to fast relaxation of electrons from higher  $5d$   $\text{Eu}^{2+}$  levels to the lowest one.

In order to demonstrate that the bands 1 and 2 are not related to europium the measurements were performed for the undoped  $\text{SrAl}_2\text{O}_4$  sample. The results are shown in Fig. 9. Both bands can be observed for the undoped sample that confirms that these bands have nothing with the presence of Eu and are probably related to the crystal structure defects. To prove this supposition the luminescence excitation spectra were measured using synchrotron radiation in a broad energy range 4–25 eV (Fig. 10). The excitation of the

intrinsic emission starts from fundamental absorption edge with the onset at 6.6 eV. First peak at 6.85 eV is related to the direct creation of excitons. High intensity of the excitation spectrum in the region from  $E_g$  and up to 13 eV indicates high efficiency of excitons creation from separated electron hole pairs, which are created when excitation energy exceeds the bandgap value. The intensity increase in the region above 15 eV is related to the multiplication of electronic excitations when one excitation photon can create two secondary excitations in the crystal. The excitation spectra of both bands 1 and 2 demonstrate excitation peaks in the region below fundamental absorption edge, i.e. in the transparency region of the crystal. It indicates that these bands can be associated with the structural

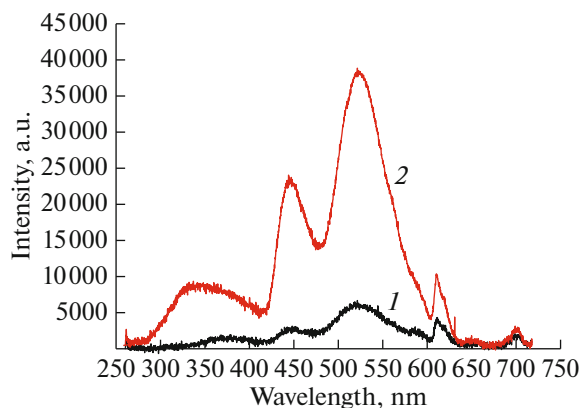


**Fig. 7.** Evolution of the cathodoluminescence spectrum from  $\text{SrAl}_2\text{O}_4:\text{Eu}^{2+}$  phosphor upon switching off the electron beam. Spectrum 1—measured at the surface from which the temperature dependence has been measured irradiation time  $\sim 3$  hours and spectrum 2—measured at the fresh part of the surface of sample.  $T = 10$  K.

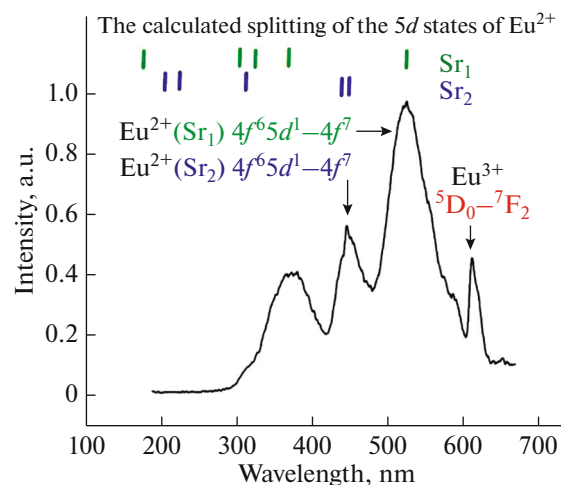


**Fig. 8.** Cathodoluminescence spectra of  $\text{SrAl}_2\text{O}_4:\text{Eu}^{2+}$  nanophosphor at  $T = 10$  K and calculated splitting of the  $5d$  states of  $\text{Eu}^{2+}$  in nanometric (nm) scale.

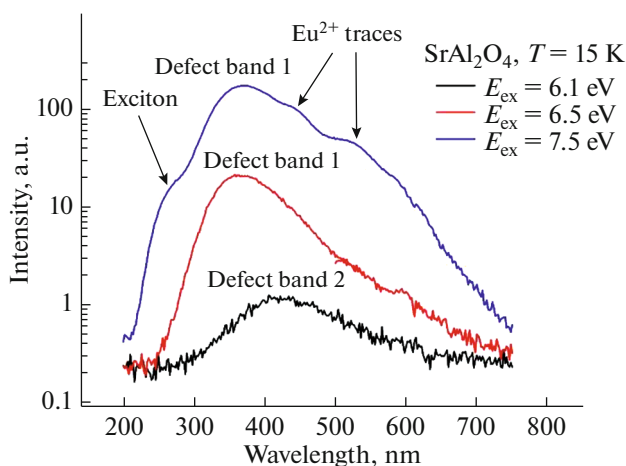


**Fig. 9.** Photoluminescence spectra of the undoped  $\text{SrAl}_2\text{O}_4$  under synchrotron radiation with different excitations:  $E_{\text{ex}} = 6.1, 6.5,$  and  $7.5$  eV at  $T = 15$  K.

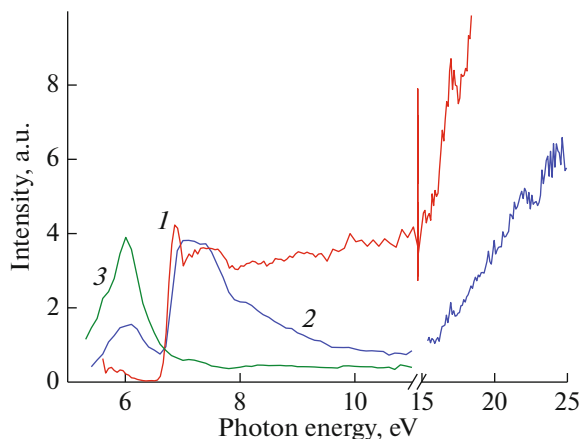


**Fig. 10.** Luminescence excitation spectra for  $\text{SrAl}_2\text{O}_4:\text{Eu}^{2+}$  measured at  $\lambda_{\text{em}} = 250$  (1), 380 (2) and 400 nm (3). Curves 1 and 2 were measured at 13 K and curve 3—at 300 K.

defects in the sample. It is worth noting that the band 2 is excited only in the transparency region of the crystal while the band 1 can be also excited via the energy transfer from the host thus demonstrating different origin of defect centers responsible for the emission bands 1 and 2.

## CONCLUSIONS

Undoped and  $\text{Eu}^{2+}$  doped  $\text{SrAl}_2\text{O}_4$  phosphors were successfully synthesized by combustion method. The details of phosphor's preparation were described and their luminescence properties were studied in broad temperature range 10–300 K. Up to six luminescence bands were detected in  $\text{SrAl}_2\text{O}_4:\text{Eu}^{2+}$  under interband and intraband excitations using synchrotron radiation as well as in cathodoluminescence experiments. The luminescence mechanism of the bands at 450 and

520 nm in  $\text{SrAl}_2\text{O}_4:\text{Eu}^{2+}$  is well known and explained as electron transitions from the lowest 5d to 4f levels of  $\text{Eu}^{2+}$  ions at  $\text{Sr}_1$  and  $\text{Sr}_2$  positions. In particular, the  $\text{Eu}^{2+}$  ions entering the  $\text{Sr}_2$  sites show broad emission at higher energy (at 450 nm), and those ions at the  $\text{Sr}_1$  sites cause the lower energy band at 520 nm. Traces of  $\text{Eu}^{3+}$  ions, which present in the sample, result in the emission with the most intensive peak at 595 nm under intraband excitation. Intrinsic emission band related to self-trapped excitons and peaking at 250 nm and two additional bands at 370 and 403 nm dominates in the emission spectrum of undoped  $\text{SrAl}_2\text{O}_4$ . Analysis of the excitation spectra of the latter two emission bands allows to ascribe them to the emission centers containing structural defects.

## FUNDING

The ANCD National Research Program (project no. 20.80009.5007.19) supported this work.

## CONFLICT OF INTEREST

The authors declare that they have no conflicts of interest.

## REFERENCES

1. T. Matsuzawa, Y. Aoki, N. Takeuchi, and Y. Murayama, *J. Electrochem. Soc.* **143**, 2670 (1996).
2. J. Hölsä, *Electrochem. Soc. Interface* **18** (4), 42 (2009).
3. K. van den Eeckhout, P. F. Smet, and D. Poelman, *Materials* **3**, 2536 (2010).
4. P. F. Smet, D. Poelman, and M. P. Hehlen, *Opt. Mater. Express* **2**, 452 (2012).
5. V. Vitola, D. Millers, I. Bite, K. Smits, and A. Spustaka, *Mater. Sci. Technol.* **35**, 14 (2019).
6. J. Botterman, J. J. Joos, and P. F. Smet, *Phys. Rev. B* **90**, 085147 (2014).
7. P. Dorenbos, *J. Lumin.* **182**, 79 (2017).
8. M. G. Brik, A. M. Srivastava, and A. I. Popov, *Opt. Mater.* **127**, 112276 (2022).
9. M. Nazarov, S. Mammadova, D. Spassky, et al., *Opt. Mater.* **75**, 448 (2018).
10. J. J. Moore and H.J. Feng, *Prog. Mater. Sci.* **39**, 243 (1995).
11. T. Balasubramanian, B. N. Jensen, S. Urpelainen, et al., *AIP Conf. Proc.* **1234**, 661 (2010).
12. H. Ji, G. Xie, et al., *J. Sol-Gel Sci. Technol.* **44**, 133 (2007).
13. P. Zhang, M. Xu, Z. T. Zeng, et al., *J. Sol-Gel Sci. Technol.* **43**, 59 (2007).
14. Y. Liu and C.-N. Xu, *J. Phys. Chem. B* **107**, 3991 (2003).
15. M. Nazarov, M. G. Brik, D. Spassky, et al., *J. Alloys Compd* **573**, 6 (2013).
16. M. Nazarov, M. G. Brik, D. Spassky, et al., *J. Lumin.* **182**, 79 (2017).